Ensemble Diffraction Microscopy: An Imaging Technique That Allows High-Resolution Diffraction Imaging Using Both Totally and Partially Coherent Sources

Ning-Jung Chen, Huai-Yu Cao, Jhih-Min Lin, Yu-Shan Huang, Yi-Wei Tsai, and Chien-Chun Chen

***Abstract*—Coherent diffraction microscopy (CDM) is a potential approach to image micromaterials at atomic resolution without crystals. Due to the lack of high-angle scattering, the achieved resolution is limited to several nanometers. Small-angle scattering allows researchers to reveal high-resolution 3D structures of specimens by fitting 1D diffraction signals. However, prerequisite 3D models and non-unique solutions restrict the potential to image general specimens. Under the assumption of an ensemble containing large amounts of identical specimens with the same orientation, the intensity distribution of the diffraction pattern of the whole ensemble is approximated to the form factor of a single specimen multiplied by the number of identical specimens. Since the diffraction intensities are contributed from the whole ensemble, the signal can be significantly extended to high-frequency regions. The feasibility of ensemble diffraction microscopy (EDM) was demonstrated by a designed sample using both totally and partially coherent X-ray sources at Taiwan Photon Source (TPS). The reconstructed images show excellent consistency with the image of a scanning electron microscope. This work represents a new protocol for directly characterizing the structures of nanomaterials, or potentially biomacromolecules, from accumulated X-ray scattering data.**

***Index Terms*—Coherent imaging, diffractive imaging, microscopy, phase-retrieval algorithm.**

I. Introduction

STRUCTURAL determination has become a crucial topic in modern science. X-ray coherent diffraction microscopy (XCDM), a methodology converting diffraction patterns to projections of specimens, is a promising method to analyze the structure without crystals [1]. Over the past few decades, XCDM has demonstrated the feasibility of revealing the inner structures of both inorganic [2], [3], [4], [5], [6] and organic microcomposites [7], [8], [9], [10], [11]. Since no spherical aberration has to be considered in this lensless setup [12], retrieving missing phases from the diffraction pattern with an appropriate oversampling ratio can be performed by an algorithm iterating back and forth between real and Fourier spaces.

The poor high-angle scattering signal of XCDM prohibits researchers from imaging specimens at a sub-nanometre resolution. It has become a bottleneck for further applications during the past two decades [13]. In order to obtain a sufficient signal-to-noise ratio at the high-frequency region (i.e., the high-q region), implanting high-Z materials, such as gold nanoparticles, into the specimen to enhance the diffraction intensities is a potential approach. Although experiments have demonstrated that the recognizable diffraction intensities can be extended to the higher-frequency region, the introduced Poisson noise might still be stronger than the signal from specimens [14], [15], [16]. The other direction is to produce brighter sources, such as X-ray free-electron lasers (XFEL), because the scattering signal is proportional to the fourth power of the flux of incidence [17], [18], [19], [20]. While the diffraction-before-destroy has been experimentally demonstrated, the resolution is still limited at a nanometre level [21]. Therefore, a more powerful light source is desired.

This article proposes an alternative method to improve the current situation. Under the assumption that a large number of identical specimens are in the same orientation, the diffraction intensities of the whole ensemble can be approximated to the form factor of a single specimen multiplied by a constant determined by the number of identical samples. The experimental demonstrations of the EDM are verified by using both partially and totally coherent beamlines at the Taiwan Photon Source (TPS).

II. Method

The theoretical basis of EDM is as follows. The scattering amplitude A(q) of an ensemble consisting of N identical particles in the same orientation is given by:

$$A(\boldsymbol{q}) = \sum_{j}^{N} f_j e^{i(\boldsymbol{q}\cdot r_j)}. \tag{1}$$

Manuscript received 8 January 2023; revised 1 March 2023; accepted 9 March 2023. Date of publication 13 March 2023; date of current version 22 March 2023. This work was supported by the Taiwan Ministry of Science and Technology under Grants 109-2112-M-007-029-MY3 and 110-2119-M-007-002-MBK. *(Corresponding authors: Yi-Wei Tsai; Chien-Chun Chen.)*

Ning-Jung Chen, Huai-Yu Cao, and Chien-Chun Chen are with the Department of Engineering and System Science, National Tsing Hua University, Hsinchu 30013, Taiwan (e-mail: shanch0527@gmail.com; hy960731@gmail.com; chenchienchun0627@gmail.com).

Jhih-Min Lin, Yu-Shan Huang, and Yi-Wei Tsai are with the National Synchrotron Radiation Research Center, Hsinchu 30076, Taiwan (e-mail: lin.jm@nsrrc.org.tw; jade@nsrrc.org.tw; tsai.yw@nsrrc.org.tw).

Digital Object Identifier 10.1109/JPHOT.2023.3256059

where q is the scattering factor, f_j presents the form factor of the jth particle in the specimen, and r_j is the coordinate of j^{th}particle [22], [23]. The scattering intensity $I(\boldsymbol{q})$ of the whole ensemble can be expressed as

$$I(\boldsymbol{q}) = A(\boldsymbol{q}) \cdot A^*(\boldsymbol{q}) = \sum_{j=1}^{N} \sum_{k=1}^{N} f_j f_k \cos\left[\boldsymbol{q} \cdot (\boldsymbol{r}_j - \boldsymbol{r}_k)\right]. \tag{2}$$

Eq. (2) can be separated into two terms, with $j = k$ for the first term and $j \neq k$ for the second term as (3).

$$I(\boldsymbol{q}) = \sum_{j=1}^{N} f_j^2 + \sum_{j=1}^{N} \sum_{\substack{k=1 \\ k \neq j}}^{N} f_j f_k \cos\left[\boldsymbol{q} \cdot (\boldsymbol{r}_j - \boldsymbol{r}_k)\right]. \tag{3}$$

Since the ensemble contains identical particles, in terms of $\boldsymbol{q} \neq 0$, the first term turns out to be Nf^2 since $f_j = f_k = f$ and $\cos\left[\boldsymbol{q} \cdot (\boldsymbol{r}_j - \boldsymbol{r}_k)\right] = 1$. The second term appears to be zero since $\langle \cos[\boldsymbol{q} \cdot (\boldsymbol{r}_j - \boldsymbol{r}_k)] \rangle = 0$ when the number of randomly distributed particles is sufficiently large. The final expression of scattering intensities is

$$I(\boldsymbol{q}) = \begin{cases} Nf^2, & j = k \\ \sim 0, & j \neq k \end{cases}. \tag{4}$$

In short, the total scattering intensity of a large number of identical particles in the same orientation is simply N times the diffraction intensity of a single particle.

III. Experiment

The proof-of-principle experiments of EDM were demonstrated at TPS 13A and TPS 25A. The beam size of the partially coherent beam at TPS 13A is 200 μm × 200 μm (coherent length ~700 nm) with an energy of 9.000 keV. The beam size of the totally coherent beam at TPS 25A is 6 μm × 8 μm with an energy of 8.838 keV. A beamstop was inserted to avoid the saturation or damage of the detector from the direct beam. An EIGER X 16M detector recorded the diffraction patterns at individual scans placed 6 meters downstream of the sample with a pixel size of 75 μm and a dwell time of 1 second (Fig. 1).

The designed specimen was composed of numerous identical tiny patterns containing alphabets I and P. All the tiny patterns are randomly distributed but aligned in the same orientation. The specimen was then deposited on a silicon nitride membrane with an area of 30 μm × 30 μm and a thickness of 100 nm by a focus ion beam system (FIB, Helios G4, Thermo Fisher Scientific) as shown in Fig. 2(a) and (b).

The data processing and reconstruction algorithm for the data acquired from 13 A and 25 A are described below. Since the EIGER detector is composed of 16 small detectors, the diffraction intensities at the gap areas between neighbor detectors and the beam stop region were missing in the experiments. After locating the origin of the diffraction pattern, we rotated the diffraction pattern by 180° and filled in the missing data according to the Friedel's law, which infers that the diffraction intensity is centrosymmetric for the object of weak absorption [24].

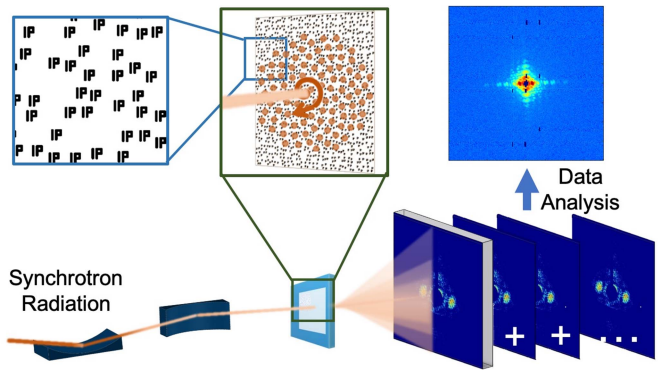

Fig. 1. Schematics of EDM experiment using third-generation synchrotron radiation. The incident beam performed Fermat's spiral scans across the designed sample deposited on a silicon nitride membrane. Multiple diffraction patterns were summarized to generate a high-resolution diffraction pattern.

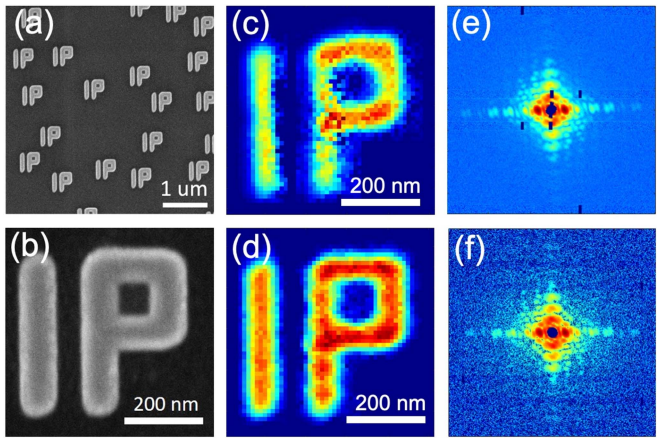

Fig. 2. The sample overview under a scanning electron microscope (SEM). (a) SEM image at a magnification of 20 k× and (b) 120 k×. The reconstructions were carried out by the guided hybrid input-output method from the diffraction patterns generated by (c) a totally coherent X-ray source and (d) a partially coherent X-ray source. The diffraction amplitudes were acquired by (e) a totally coherent X-ray source and (f) a partially coherent X-ray source.

The guided hybrid-input-output (GHIO) algorithm [25] was employed to perform the phase retrieval (Fig. 3). Based on the HIO algorithm [26], we first performed 100 independent reconstructions from 100 random initial phases. For each reconstruction, the best result was selected during the 500 HIO iterations while the initial support size was estimated from the distance of circular fringes in the diffraction pattern. A tight support was then determined from the average of 100 independent reconstructions. Next, a set of 100 new independent reconstructions (so-called the first generation) was obtained when the tight support was applied. We averaged all 100 reconstructions to generate a reference image. A guided image was calculated by taking the geometric average of the individual reconstructions and the reference image accordingly. When the inverse Fourier transform was applied to the individual guided images, the phases can be used as the initial phases for a new set of reconstructions (so-called the second generation). We repeated the same procedure for all 100 reconstructions until

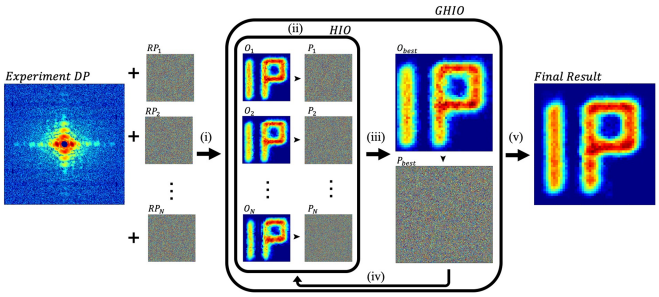

Fig. 3. Flowchart of guided hybrid-input-output (GHIO). (i) The diffraction pattern (DP) obtained by the experiment is combined with N initial random phases (RP) independently. (ii) Executing conventional HIO algorithm to obtain N individual reconstructions of the object (O). O's phase (P) is then obtained by applying the Fourier transform. (iii) For each reconstruction, the best result ($\boldsymbol{O_{best}}$) was selected during the HIO iterations. The corresponding phase ($\boldsymbol{P_{best}}$) is also obtained from the Fourier transform of $\boldsymbol{O_{best}}$. (iv) Guiding the reconstruction by calculating the geometric average of the individual reconstructions and the reference image, then repeating the HIO iterations. (v) The final reconstruction is obtained after no improvement is observed.

no improvement could be observed. The final reconstructions in the totally and partially coherent experiments are depicted in Fig. 2(c) and (d).

IV. Results and Discussions

Fig. 4(a) shows the diffraction pattern produced by a coherent X-ray source at a single position. The fringe inside the speckle [27] is visible, contributed by the interference from tiny IP patterns within the beam area. Under an equivalence exposure time of 200 s, the estimated spatial resolution of the diffraction intensity is about 39.10 nm (green circle in Fig. 4(a)) [28]. After summing 6602 patterns, Fig. 4(b) shows that the fringes inside the speckle are invisible for both cases indicating that the position distribution of tiny IP patterns has been averaged out. The spatial resolution of the diffraction intensity has improved to about 25.89 nm (white circle in Fig. 4(b) and (d)). Fig. 4(c) shows the diffraction pattern collected by a partially coherent beam under the same exposure time as Fig. 4(a) and (d) shows the summed diffraction patterns at all incident positions in the partially coherent experiments. After being summarized, the spatial resolution was also improved to 25.89 nm. All the patterns are cropped into 1001×1001 pixels such that the estimated pixel resolutions from the cropped diffraction patterns are 11.04 and 11.25 nm in the case of partial and total coherence, respectively [29].

The final reconstructions from totally and partially coherent experiments were generated by averaging the best 20 out of 100 reconstructed images in the GHIO process [16]. The density distributions of two reconstructed images show an excellent agreement with the design. We divided all diffraction patterns into two groups to calibrate the reconstructed resolution and then obtained the reconstruction from the summed diffraction pattern generated in each group. The reconstructions from two independent datasets can be used to calculate the consistency by Fourier shell correlation (FSC) [30], which has been widely used to estimate the resolution in the community of cryogenic

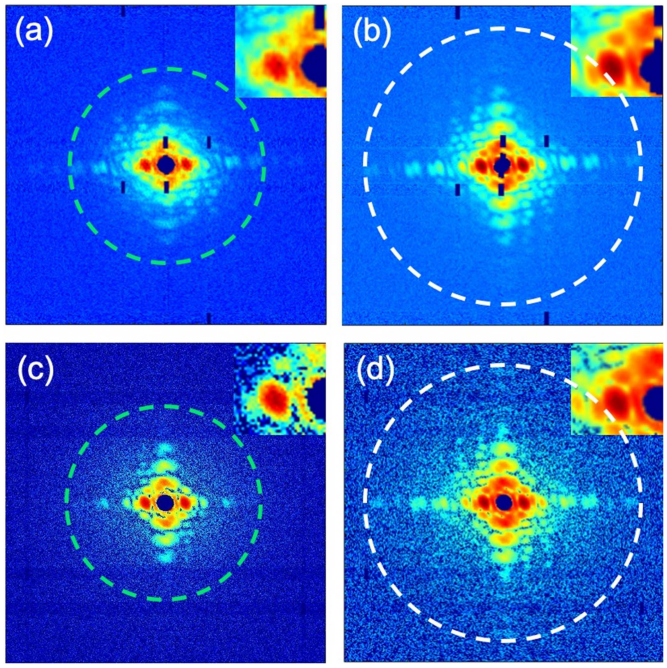

Fig. 4. Comparison of single-exposure and accumulated diffraction patterns. (a) The diffraction pattern of one single position was collected under a totally coherent X-ray for an exposure time of 200s (TPS 25A). The fringe inside the speckle is visible, indicating that the interference of tiny IP patterns is not negligible. The green circle shows the approximate scattering range with a spatial resolution of 39.10 nm. (b) Summed diffraction pattern after scanning along a Fermat's spiral trajectory on the whole sample under a totally coherent X-ray. Overall exposure time is 6602s. The white circle shows the approximate scattering range with a spatial resolution of 25.89 nm. (c) The diffraction pattern of one single position was collected under a partially coherent X-ray for the same exposure time of (a). (d) Summed diffraction pattern by a partially coherent X-ray (TPS 13A) with background deduction and an overall exposure time of 6020 s. In (d), data were collected without moving the sample stage since the beam size is larger than the whole sample area.

electron microscopy. As shown in Fig. 5(c) and (d), the spatial resolutions of the retrieved images are 45.45 nm and 45.87 nm with a T1-bit threshold, respectively.

To quantify the improvement of resolution by accumulating the diffraction patterns, the FSC of Fig. 4(a) and (c) were also calculated by the same process described above. Fig. 5(a) and (c) show the spatial resolutions are 60.24 nm and 79.37 nm with a T1-bit threshold, respectively. The results demonstrate that the interference of tiny IP patterns in experiments can be averaged out by accumulating the diffraction patterns. The spatial resolution can be significantly improved in both cases.

In the final of result and discussion, EDM is compared with other X-ray diffraction imaging methods. Conventional CDI requires a highly coherent source, and the beam size must be larger than the sample of interest. In Ptychography, the partial coherence effect in the reconstruction can be improved by a mulit-mode approach. Besides, the resolution is usually limited due to the weak scattering signals from an isolated sample. Although ptychography allows imaging of an extended sample which has a broader application than CDI, the resolution in Ptychography has no improvement due to the poor scattering efficiency of X-rays. The beamstop size and the oversampling

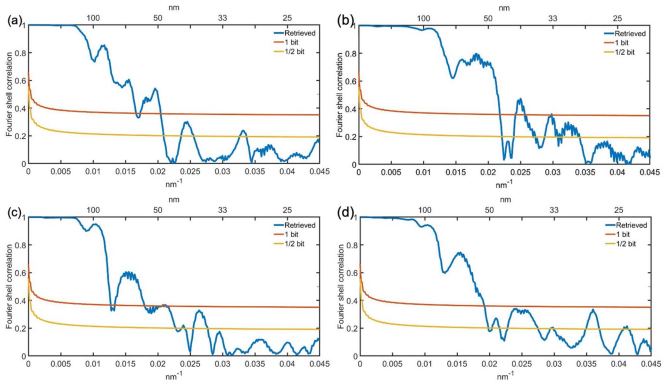

Fig. 5. Comparison of reconstructed resolution from single-exposure and accumulated diffraction patterns using the Fourier shell correlation (FSC) with T1-bit threshold. (a) FSC of the totally coherent experiment at TPS 25A with a data acquiring equivalence time of 200 s, and the spatial resolution is 60.24 nm. (b) After summarizing the diffraction patterns with an equivalence time of 6602 s, the resolution achieves 45.87 nm. (c) FSC of the partially coherent experiment at TPS 13A with a data acquiring equivalence time of 200 s, and the spatial resolution is 79.37 nm. (d) After summarizing the diffraction patterns with an equivalence time of 6020 s, the resolution achieves 45.45 nm.

ratio are critical to the CDI reconstruction, while ptychography significantly bypasses the limitation. In our demonstration, the advantages of EDM are three-fold. First, the requirement for coherence is not demanding. Both totally and partially coherent sources can apply to obtain correct reconstructed images. Second, the form factor of a tiny sample contributes to the high-q region, while the low-q part contains the information on sample distribution. This geometry allows a much larger missing center and usually provides a significantly sizeable oversampling ratio. Third, accumulating the diffraction patterns dramatically enhances the signal-to-noise ratio (SNR) in the high-q area, giving great potential for imaging small high-resolution samples.

V. Conclusion

In conclusion, we have demonstrated EDM through both theory and experiments. The images were successfully reconstructed at a spatial resolution of ∼45 nm by utilizing totally and partially coherent X-ray sources. Compared to conventional small angle X-ray scattering and coherent diffraction microscopy, EDM provided a high-resolution direct imaging protocol without prior knowledge. With the advance of the schemes regarding sample alignment, this technique is anticipated to find broad applications to nanomaterials and biomacromolecules using synchrotron radiation sources and free-electron lasers.

Acknowledgment

The authors would like to thank TPS 13A for the beamtime, and the staff of the beamline for assisting with data collection by a partially coherent X-ray source.

References

[1] J. Miao, P. Charalambous, J. Kirz, and D. Sayre, "Extending the methodology of X-ray crystallography to allow imaging of micrometre-sized non-crystalline specimens," *Nature*, vol. 400, no. 6742, pp. 342–344, 1999.

[2] I. K. Robinson, I. A. Vartanyants, G. J. Williams, M. A. Pfeifer, and J. A. Pitney, "Reconstruction of the shapes of gold nanocrystals using coherent X-ray diffraction," *Phys. Rev. Lett.*, vol. 87, no. 19, 2001, Art. no. 195505.

[3] J. Miao, T. Ishikawa, B. Johnson, E. H. Anderson, B. Lai, and K. O. Hodgson, "High resolution 3D X-ray diffraction microscopy," *Phys. Rev. Lett.*, vol. 89, no. 8, 2002, Art. no. 088303.

[4] M. A. Pfeifer, G. J. Williams, I. A. Vartanyants, R. Harder, and I. K. Robinson, "Three-dimensional mapping of a deformation field inside a nanocrystal," *Nature*, vol. 442, no. 7098, pp. 63–66, 2006.

[5] G. J. Williams et al., "Fresnel coherent diffractive imaging," *Phys. Rev. Lett.*, vol. 97, no. 2, 2006, Art. no. 025506.

[6] P. Thibault, M. Dierolf, A. Menzel, O. Bunk, C. David, and F. Pfeiffer, "High-resolution scanning X-ray diffraction microscopy," *Science*, vol. 321, no. 5887, pp. 379–382, 2008.

[7] A. Tripathi et al., "Dichroic coherent diffractive imaging," *Proc. Nat. Acad. Sci.*, vol. 108, no. 33, pp. 13393–13398, 2011.

[8] D. Shapiro et al., "Biological imaging by soft X-ray diffraction microscopy," *Proc. Nat. Acad. Sci.*, vol. 102, no. 43, pp. 15343–15346, 2005.

[9] C. Song et al., "Quantitative imaging of single, unstained viruses with coherent X rays," *Phys. Rev. Lett.*, vol. 101, no. 15, 2008, Art. no. 158101.

[10] Y. Nishino, Y. Takahashi, N. Imamoto, T. Ishikawa, and K. Maeshima, "Three-dimensional visualization of a human chromosome using coherent X-ray diffraction," *Phys. Rev. Lett.*, vol. 102, no. 1, 2009, Art. no. 3018101.

[11] K. Giewekemeyer et al., "Quantitative biological imaging by ptychographic X-ray diffraction microscopy," *Proc. Nat. Acad. Sci.*, vol. 107, no. 2, pp. 529–534, 2009.

[12] H. N. Chapman and K. A. Nugent, "Coherent lensless X-ray imaging," *Nature Photon.*, vol. 4, no. 12, pp. 833–839, 2010.

[13] J. Miao, J. E. Amonette, Y. Nishino, T. Ishikawa, and K. O. Hodgson, "Direct determination of the absolute electron density of nanostructured and disordered materials at sub-10-nm resolution," *Phys. Rev. B*, vol. 68, no. 1, 2003, Art. no. 012201.

[14] C. Kim et al., "Resolution enhancement in coherent X-ray diffraction imaging by overcoming instrumental noise," *Opt. Exp.*, vol. 22, no. 23, 2014, Art. no. 29161.

[15] T.-Y. Lan, P.-N. Li, and T.-K. Lee, "Method to enhance the resolution of X-ray coherent diffraction imaging for non-crystalline bio-samples," *New J. Phys.*, vol. 16, no. 3, 2014, Art. no. 033016.

[16] J.-H. Yang, N.-J. Chen, Y. K. Hwu, and C.-C. Chen, "Algorithm for characterizing the subcellular structures of nanometer-sized biological specimens in a solution using X-ray free-electron lasers," *Phys. Rev. Mater.*, vol. 3, no. 12, 2019, Art. no. 123803.

[17] H. N. Chapman et al., "Femtosecond diffractive imaging with a soft-X-ray free-electron laser," *Nature Phys.*, vol. 2, no. 12, pp. 839–843, 2006.

[18] M. M. Seibert et al., "Single mimivirus particles intercepted and imaged with an X-ray laser," *Nature*, vol. 470, no. 7332, pp. 78–81, 2011.

[19] R. P. Kurta et al., "Correlations in scattered X-ray laser pulses reveal nanoscale structural features of viruses," *Phys. Rev. Lett.*, vol. 119, no. 15, 2017, Art. no. 158102.

[20] A. T. Young, "Rayleigh scattering," *Appl. Opt.*, vol. 20, no. 4, pp. 533–535, 1981.

[21] T. Kimura et al., "Imaging live cell in micro-liquid enclosure by X-ray laser diffraction," *Nature Commun.*, vol. 5, no. 1, 2014, Art. no. 3052.

[22] L. A. Feigin and D. I. Svergun, *Structure Analysis by Small-Angle X-Ray and Neutron Scattering*. New York, NY, USA: Plenum Press, 1987.

[23] H. Brumberger, "Modern aspects of small-angle scattering," in *Proc. NATO Adv. Study Inst. Modern Aspects Small-Angle Scattering*, 1993, pp. 1–56.

[24] I. A. Vartanyants and I. K. Robinson, "Partial coherence effects on the imaging of small crystals using coherent X-ray diffraction," *J. Phys.: Condens. Matter*, vol. 13, no. 47, pp. 10593–10611, 2001.

[25] C.-C. Chen, J. Miao, C. Wang, and T. Lee, "Application of optimization technique to noncrystalline X-ray diffraction microscopy: Guided hybrid input-output method," *Phys. Rev. B*, vol. 76, no. 6, 2007, Art. no. 064113.

[26] Y. Nishino, J. Miao, and T. Ishikawa, "Image reconstruction of nanostructured nonperiodic objects only from oversampled hard X-ray diffraction intensities," *Phys. Rev. B*, vol. 68, no. 22, 2003, Art. no. 220101.

[27] Y. Chushkin and F. Zontone, "Upsampling speckle patterns for coherent X-ray diffraction imaging," *J. Appl. Crystallogr.*, vol. 46, no. 2, pp. 319–323, 2013.

[28] M. R. Piggott, "Resolution of diffraction rings by X rays and electrons," *J. Appl. Phys.*, vol. 37, no. 7, pp. 2927–2927, 1966.

[29] N. Burdet et al., "Observations of artefacts in the X-ray ptychography method," *Opt. Exp.*, vol. 22, no. 9, 2014, Art. no. 10294.

[30] M. van Heel and M. Schatz, "Fourier shell correlation threshold criteria," *J. Struct. Biol.*, vol. 151, no. 3, pp. 250–262, 2005.